Operational control strategy on optimal calcium removal in drinking water treatment processes

Insights from reactor experiments, modelling and particle characterization

Seepma, Sergěj Y.M.H.; Koskamp, Janou A.; Colin, Michel G.; Chiou, Eleftheria; Sobhan, Rubayat; Bögels, Tim F.J.; Bastiaan, Tom; Zamanian, Hadi; Baars, Eric T.; de Moel, Peter J.

DOI
10.1016/j.watres.2025.123647

Publication date
2025

Document Version
Final published version

Published in
Water Research

Citation (APA)
Seepma, S. Y. M. H., Koskamp, J. A., Colin, M. G., Chiou, E., Sobhan, R., Bögels, T. F. J., Bastiaan, T., Zamanian, H., Baars, E. T., de Moel, P. J., Wolthers, M., & Kramer, O. J. I. (2025). Operational control strategy on optimal calcium removal in drinking water treatment processes: Insights from reactor experiments, modelling and particle characterization. *Water Research*, *282*, Article 123647. https://doi.org/10.1016/j.watres.2025.123647

Water Research 282 (2025) 123647

Contents lists available at ScienceDirect

Water Research

journal homepage: www.elsevier.com/locate/watres

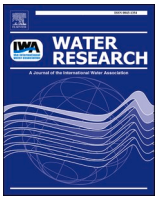

Operational control strategy on optimal calcium removal in drinking water treatment processes: Insights from reactor experiments, modelling and particle characterization

Sergĕj Y.M.H. Seepma [*,a,b,1], Janou A. Koskamp [a], Michel G. Colin [b], Eleftheria Chiou [b,c,2], Rubayat Sobhan [b,c,3], Tim F.J. Bögels [a,b,4], Tom Bastiaan [a,b,5], Hadi Zamanian [b], Eric T. Baars [b], Peter J. de Moel [b,e], Mariëtte Wolthers [*,a], Onno J.I. Kramer [*,b,c,d]

[a] Utrecht University, Department of Earth Sciences, Princetonlaan 8A, 3584 CB Utrecht, the Netherlands
[b] Waternet, PO Box 94370, 1090 GJ, the Netherlands
[c] Delft University of Technology, Faculty of Civil Engineering and Geosciences, Department of Water Management, PO Box 5048, 2600 GA, Delft, the Netherlands
[d] Queen Mary University of London, School of Engineering and Materials Science, Division of Chemical Engineering, Centre for Sustainable Engineering, Mile End Road E1 4NS, London, United Kingdom
[e] Omnisys, Eiberlaan 23, 3871 TG Hoevelaken, the Netherlands

ARTICLE INFO

Keywords:
Multiphase flow systems
Mixing dynamics
Reactor engineering
Water softening
Calcium removal
$CaCO_3$ precipitation kinetics

ABSTRACT

Drinking water softening is an essential treatment step that provides multiple benefits, including public health, reduction of environmental impact, decrease in clogging potential and improvement in heating efficiency. With approximately 35 billion cubic meters of water being softened annually worldwide, the predominant methods are conventional lime/soda-ash softening, nanofiltration, ion exchange, and seeded crystallization through pellet-water softening. This study addresses the limitations in existing predictive models for calcium carbonate ($CaCO_3$) precipitation kinetics in industrial-scale pellet-water softening by experimentally investigating the integral and multivariate effects of particle-, fluid-, water matrix- and reactor properties, on $CaCO_3$ precipitation kinetics. Fluid characterization experiments were conducted at lab-scale continuous-stirred tank reactors (CSTR), pilot-scale plug-flow reactors (PFR), and full-scale fluidized bed reactors (FBR) at the Waternet Weesperkarspel treatment plant in Amsterdam, The Netherlands. In parallel, solid characterization was performed with image analysis software on pellets and SEM on fines extracted from water samples, where both pellet and water samples were collected during FBR experiments. The calcium removal data obtained from experiments were compared with modeled $CaCO_3$ precipitation rates using and extending the most recently developed water softening model for pellet-water softening. The results predominantly highlight the critical role of mixing dynamics — between softening chemicals, hard influent water and seeding material — for accurate $CaCO_3$ precipitation predictions across various reactor types and other reactor-specific properties such as the residence time of influent hard water. Additional enhancements can be achieved by targeting fluid properties, followed by water matrix properties, and finally particle properties, though these factors exhibit a progressively smaller impact on overall water softening improvement. By implementing these prioritized optimization strategies, the operational control strategy for calcium removal will be enhanced, leading to improvements in cost-effectiveness, sustainability, and reliability in drinking water treatment processes.

* Corresponding author at: Utrecht University, Department of Earth Sciences, Princetonlaan 8A, 3584 CB Utrecht, the Netherlands.
E-mail address: s.y.m.h.seepma@uu.nl (S.Y.M.H. Seepma).
[1] IA Group, Geograaf 40, 6921 EW Duiven, The Netherlands.
[2] Hoogheemraadschap van Rijnland, Breestraat 59, 2311 CJ Leiden, The Netherlands.
[3] Deutsche Gesellschaft für Internationale Zusammenarbeit, 89 Gulshan Ave, Simpletree Anarkali, Dhaka, Bangladesh.
[4] Université de Paris, Institut de Physique de Globe de Paris, 75005 Paris, France.
[5] Vitens, Oude Veerweg 1, 8019 BE Zwolle, The Netherlands.

https://doi.org/10.1016/j.watres.2025.123647
Received 22 January 2025; Received in revised form 27 March 2025; Accepted 12 April 2025
Available online 13 April 2025

Nomenclature

Acronyms

AOC	Assimilable organic carbon
CC	Crushed calcite
CP	Calcite pellets
CRES	Corrosion-resistant steel
CSTR	Continuous-stirred tank reactor
EC	Electrical conductivity
EOP	Experimental operating procedure
FBR	Fluidized bed reactor
ISE	Ion selective electrode
KPI	Key reactor performance indicator
PFR	Plug-flow reactor
SA	Surface area
SEM	Scanning electron microscopy
TOC	Total organic carbon
WPK	Waternet Weesperkarspel drinking water treatment plant in Amsterdam, The, Netherlands

Symbols

$CCPP_{rel}$	Relative theoretical calcium carbonate precipitation potential, –
D_r	Cylindrical vessel diameter of pellet softening reactor, m
d_{ch}	(Average) channel diameter between two adjacent particles, m
d_{im}	Impeller diameter, m
d_p	(Average) particle diameter of calcite pellets, m
D_f	Diffusion coefficient, $m^2\ s^{-1}$
f_r	Recrystallization factor, –
h_r	Fluidized bed height, m
J_p, J_c, J_n	Precipitation, crystallization, nucleation molar rate, mol $m^{-3}\ s^{-1}$
K_c	Mass transfer coefficient, m s^{-1}
m_s	Total solid mass, kg
ϕ_s	Solid volume fraction, –
r_{aq}	Solution stoichiometry, –
r	Kinetic rate, mol $m^{-3}\ s^{-1}$
SA	Total surface area, m^2
SI_{cal}	Saturation index of calcite, –
SSA_M	Specific surface area per mass, $m^2\ kg^{-1}$
SSA_R	Specific surface area per reactor volume, $m^2\ m^{-3}$
SSA_W	Specific surface area per water volume, $m^2\ m^{-3}$
SSV	Specific space velocity, s^{-1}
T	Temperature, °C or K
t_m	Mixing time to achieve homogeneous particle-fluid system, s
t_r	Reaction time (of the ongoing $CaCO_3$ precipitation reaction), s
v_s	Linear superficial fluid velocity, m s^{-1}
V_s	Total volume, m^3

Greek Symbols

ε	Bed voidage, –
μ	Dynamic viscosity, kg $m^{-1}\ s^{-1}$
ν_k	Kinematic viscosity, $m^2\ s^{-1}$
ρ_f, ρ_s	Density of the fluid or solid respectively, kg m^{-3}
τ_r	(Average) water residence time, s
χ_s	Morphological particle shape factor, –
Ω_{cal}	Saturation degree with respect to calcite, –

Dimensionless numbers

Re_ε	Voidage Reynolds number, $\rho_f v_s d_{ch}/\mu(1-\varepsilon)$
Sc	Schmidt number, ν_k/D_f
Sh	Sherwood number, $(0.5Re_\varepsilon^{0.5} + 0.2Re_\varepsilon^{0.667})Sc^{0.333}$

1. Introduction

Drinking water treatment includes a series of filtration, absorption, nucleation, crystallization, and fluidization processes prior to distribution to consumers, where drinking water softening is an essential treatment step (Hofman et al., 2006; Kramer, 2021). It is beneficial for public health (Tang et al., 2019), the environment (Watkinson, 2008), social costs (Van der Bruggen et al., 2009), and client comfort (Mons et al., 2007; Mitchell, 2008). Currently, more than 35 billion cubic meters of water is softened worldwide per year and this volume continues to increase (Eke et al., 2020). The predominant methods used in water softening are conventional lime/soda-ash softening using gravity clarifiers, nanofiltration, ion exchange, and pellet-water softening through seeded crystallization within fluidized bed reactors (FBRs). Of these, pellet-based softening has emerged as the prevailing method (Hofman et al., 2006). Pellet-water softening typically uses cylindrical FBRs filled with seeding material that is fluidized due to water upflow (Crittenden et al., 2012). Depending on the water alkalinity and the composition of the hardness-causing ions, the water softening process involves the precipitation of $CaCO_3$ (calcite) via the addition of NaOH (caustic soda), $Ca(OH)_2$ (lime) or Na_2CO_3 (soda ash) (Hofman et al., 2006; Van der Bruggen et al., 2009). Water softening by addition of NaOH is represented by the following representative chemical equation:

$$NaOH\ (aq) + Ca^{2+}(aq) + HCO_3^-(aq) \rightarrow CaCO_3\ (s)\downarrow + Na^+(aq) + H_2O(l) \quad (1)$$

The industrial pellet-water softening process has undergone significant modifications over the last decades to optimize the process's control, environmental emissions, circularity and costs (Barrios et al., 2008; Van der Bruggen et al., 2009; Palmen et al., 2014; Schetters et al., 2015). Major improvements often include the replacement of Australian-sourced garnet sand, widely used as seeding material in pellet reactors for calcium removal due to its relatively high density, by more locally-sourced and often relatively lower density material, such as reusable calcite pellets (Barrios et al., 2008; Schetters, 2013; Schetters et al., 2015). As a result, progress was made towards transforming the drinking water softening process from a linear to a more circular system (Palmen et al., 2014; Schetters et al., 2015; Tang et al., 2019). In addition, this transition led to improved softening affinity conditions, due to the more similar atomic arrangement between the calcite pellets and the crystal lattice formed around the pellets, during $CaCO_3$ crystallization (Lin and Singer, 2005a). Moreover, the bed voidage (ε) prediction was recently improved, where it is now linked to (macro-scale) multiphase characteristics (Kramer, 2021), rather than relying solely on the terminal settling velocity of particles (Richardson and Zaki, 1954) or minimum fluidization conditions (Kozeny, 1927; Carman, 1937). On top of that, site-specific improvements have often been implemented. Despite operational changes and process adjustments, pellet-water softening is not yet operating at optimized conditions, as it fails to achieve the $CaCO_3$ thermodynamic equilibrium during the softening process. This results in reduced overall water quality and sustainability, as well as compromised safety standards due to the physical maintenance work required for scraping and cleaning softening reactors and downstream equipment. In addition, there are unnecessary high costs associated with softening chemical usage and plant-wide maintenance. It also leads to increased downtime due to maintenance, and reduced process flexibility due to the need for more active process control. Furthermore, these issues hinder progress in the development and improvement of reactor

design and process control strategy. Currently, there is no academic and scientific evidence of how these operational and process modifications affect the calcium removal performance during pellet-water softening.

In addition, there remains significant potential to enhance the kinetic modeling of calcium removal during pellet-water softening. Current models are often based on localized geographic and instrumental settings, assume instantaneous and homogeneous mixing of softening chemicals, influent hard water, and seeding material (Nijssen et al., 2021), and involve linear calcium carbonate crystallization kinetics (Rietveld, 2005; Van Schagen et al., 2008). Earlier studies established that calcium removal through crystallization depends on the Ca^{2+} and CO_3^{2-} concentrations and the total surface area of the seeding material (pellets) (Nancollas and Reddy, 1971; Reddy and Nancollas, 1971; Wiechers et al., 1975). However, these studies did not take into account the separation between desirable heterogeneous crystallization onto the seed material and undesirable homogeneous nucleation of $CaCO_3$ into the fluid phase. Yet, this separation is essential, especially with regards to the operational and maintenance costs of downstream treatment processes. Recent research (Seepma et al., 2025) has incorporated this separation into a new calcium removal model, alongside efforts to overcome the limitations of localized settings. Nonetheless, model validation has so far been restricted to a single reactor type, leaving its broader applicability to diverse reactor configurations and operating conditions unexplored, thereby limiting its potential in improving operational strategies.

To address the operational and modeling knowledge gaps, we investigated the impact of various environmental and process conditions on the $CaCO_3$ precipitation kinetics during pellet-water softening experimentally and extended Seepma et al. (2025)'s modeling approach to account for different reactor configurations. This was achieved through a series of experiments conducted in three different reactor types, thereby addressing the impact of reactor properties. In these experiments, temperature, particle size, fluid velocity and (initial) degree of supersaturation with respect to calcite, were systematically varied. This approach allowed us to test a broad range of physical and chemical conditions across the different reactor types. In addition, the effect of ozonation prior to water softening as well as inhibition by Mg, PO_4, SO_4, and total organic carbon (TOC) on $CaCO_3$ precipitation kinetics were experimentally investigated. Furthermore, water and pellet samples during the FBR experiments were extracted and analyzed with regards to changes in calcite pellet (CP) size and shape during softening and to characterize $CaCO_3$-nucleated fines, respectively. The modeling knowledge gap was addressed through comparison of our experimental data with model predictions by employing Seepma et al. (2025)'s mechanistic model approach and through model modifications to account for different reactor configurations, addressing the model's flexibility in future reactor design applications.

Our multi-scale approach — from reaction-controlled conditions at lab-scale continuous-stirred tank reactor (CSTR) and transport-limited conditions at pilot-scale plug-flow reactor (PFR) to more balanced conditions in full-scale fluidized bed reactor (FBR), combined with model predictions for comparative analysis, as well as pellet and $CaCO_3$ particle fines characterization — allows for an integral qualitative impact assessment of the various physicochemical process parameters that influence the $CaCO_3$ removal performance. This study provides new insights into design, improvement, and operational strategies for pellet-water softening, focusing on maximizing desirable crystallization and minimizing undesirable homogeneous nucleation. Ultimately, these insights contribute to improving the reliability, circularity and sustainability of drinking water production.

2. Materials and methods

The CSTR experiments were conducted at laboratory scale to provide high control and resolution of process variables, allowing for a detailed study of the precipitation kinetics. These experiments allowed for the independent investigation of respectively the impact of specific surface area per unit volume of water (SSA_W) and temperature (T) on the precipitation kinetics across a wider range of process conditions compared to PFR and FBR. While PFR experiments resembled practical applications by balancing parameter control with the ability to investigate a wide range of experimental variables, such as T and pellet diameter (d_p), they are less effective in isolating and analyzing the specific impact of SSA_W compared to CSTR experiments. Conversely, FBR experiments provide insights under full-scale operational conditions, capturing the influence of practical uncertainties and upscaling effects characteristic of real-world applications. It is important to note that the flow dynamics in CSTR are dominated by the impeller velocity and reactor dimensions, resulting in a more turbulent flow regime. Conversely, in PFR and FBR systems, flow dynamics are less turbulent, where particle properties have a more significant impact on the system's flow and mass transfer behaviour. The use of these three reactor types enabled the investigation of the mixing time (t_m) across a series of estimated ranges: 0.1–1 s in CSTR, 1–10 min in PFR and 10–60 s in FBR. The selection of process conditions used for each experiment in this study was based on appropriate model ranges for academic purposes, conditions found in softening practices and those found locally at the Waternet Weesperkarspel treatment plant in Amsterdam, The Netherlands (WPK) where our experiments were conducted (Supplementary Information (SI)-I). In the following subsections, the experimental setup for each type of reactor is addressed, where the detailed experimental operating procedure (EOP) is found in SI-II. In Section 2.4 and 2.5, the general data handling and the specific adjustments made to Seepma et al. (2025)'s model to accommodate for varying reactor type conditions are discussed.

2.1. Continuous-stirred tank reactor experiments

CSTR experiments were conducted with 1 L volume of WPK non-ozonated influent hard water extracted from the drinking water treatment plant. A typical composition for this WPK water is found in SI-III. For seeded CSTR experiments, $CaCO_3$ Merck powder was subsequently added to the CSTR reactor before the addition of NaOH (SI-IV). Different total masses of $CaCO_3$ powder (m_s), ranging from 0 (unseeded) to 60 g, were used in the experiments to investigate the effect of surface area on the softening process. m_s is directly proportional to the total surface area (SA) available for crystallization. Besides at different m_s-loads, CSTR experiments were also conducted at three distinct temperatures; $T = 5$, 20 and 40 °C. While $T = 40$ °C is not representative of standard drinking water softening treatment conditions, elevated temperatures are more commonly observed in industrial softening reactors (Zhang et al., 2020). Therefore, this study included $T = 40$ °C to assess the impact of T across a broader range, examine whether the impact on the softening performance is linear or non-linear, and identify potential operational limitations within our experimental set-up or approach.

To facilitate comparison of SSA_W among the three types of reactor experiments, the SSA_W in CSTR was calculated based on m_s. According to Nilsson and Sternbeck (1999), the specific surface area per mass (SSA_M) for this type of $CaCO_3$ powder was estimated at 0.348 ± 0.004 $m^2\ g^{-1}$, using the BET method with N_2 gas adsorption. This information was used to calculate other relevant hydrodynamic process conditions (see SI-V for the calculation methods), such that the different experiments could be compared. In addition, the particle size distribution was measured by laser diffraction (SI-VI) and compared with the calculated (average) particle size. This comparison contributes to the accuracy of SSA_W. The corresponding values are found in Table 1.

The CSTR set-up is shown in Fig. 1a. During the CSTR experiments, pH (±0.1 pH-unit, see SI-VII) and electrical conductivity (EC) were measured continuously at an interval of 1 s. In addition, both electrodes measured temperature with an accuracy of ± 0.1 °C. The stirrer was set at approximately 1000 rpm. Each CSTR experiment continued for at least four minutes, matching the (average) residence time of influent hard water during industrial pellet-water softening.

Table 1
Hydrodynamic process conditions. Note that, for model calculations, $m_s = 0.01$ g/L was assumed when no $CaCO_3$ was used to account for naturally present particulate matter and is a reasonable value according to Burton et al. (2013).

m_s [g L^{-1}]	V_s [cm^3]	ϕ_s [–]	ε [–]	SA [m^2]	SSA_R [m^2 m^{-3} reactor]	SSA_W [m^2 m^{-3} H_2O]	Calculated d_p [μm]	Measured d_p [μm]
0	0	0	1	0	0	0	0	0
1	0.369	0.000369	> 0.999	0.348	348	348	6.362	26.3
5	1.845	0.00185	0.998	1.74	1740	1743	6.362	26.3
10	3.690	0.00369	0.996	3.48	3480	3493	6.362	26.3
30	11.07	0.0111	0.989	10.44	10,440	10,557	6.362	26.3
60	22.14	0.0221	0.978	20.88	20,880	21,353	6.362	26.3

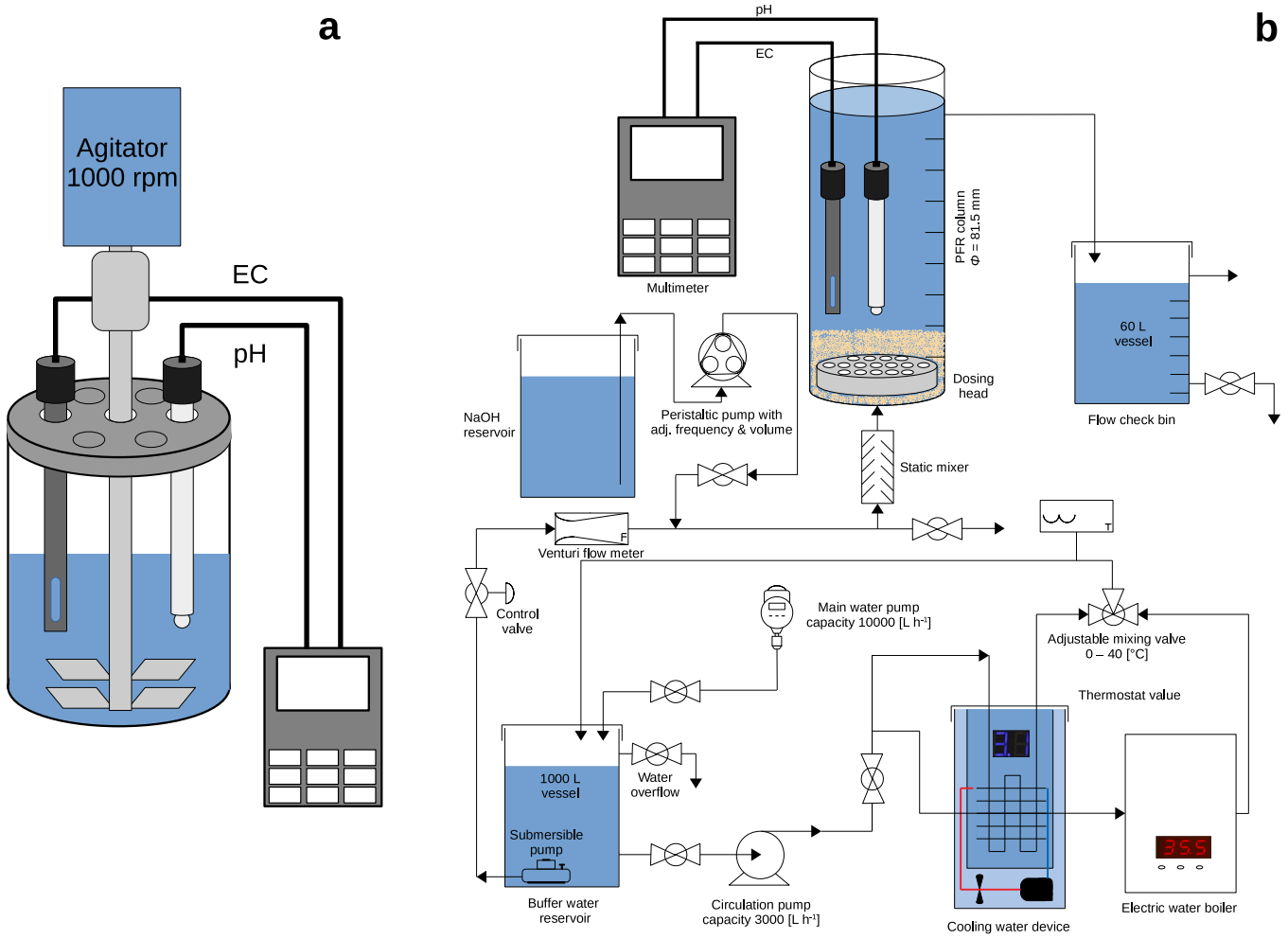

Fig. 1. Continuous-stirred tank reactor (a) and plug-flow reactor (b) experimental set-up.

2.2. Plug-flow reactor experiments

PFR experiments were carried out with the same WPK water as in the CSTR experiments (see SI-III). In addition, experiments were conducted with ozonated WPK water. These experimental results were compared and aimed to assess if pre-softening treatment processes, such as ozonation, impact the effectiveness of the subsequent softening process. Ozonation does not affect the concentrations in the water matrix significantly, but breaks down larger organic molecules to small organic molecules that may affect calcite precipitation (Meldrum and Cölfen, 2008). Furthermore, PFR experiments were performed with CP, rather than the $CaCO_3$ powder that was used in CSTR. This use of CP was adopted to prevent entrainment of fine particles into the effluent and to better simulate industrial-scale conditions. The particle size distribution for the sieved CP fraction of 1.00 – 1.12 mm, which was used in each PFR experiment, is found in SI-VIII.

The PFR experiments were performed in a transparent PVC column, with a column diameter $D_r = 81$ mm and a column height of 880 mm, at which the water outlet was positioned. The PFR experimental set-up is found in Fig. 1b. The incoming water was temperature-conditioned in an IBC tank (~1000 L in volume) and flowed with circa 420 L h^{-1}, resembling full-scale conditions of $v_s = 80$ m h^{-1}. NaOH addition was established by a peristaltic dosing and metering pump. The pH and EC electrodes were initially positioned about 50 mm above the dosing head and recorded measurements at a five-second interval. Throughout continuous operation, additional CP-layers were added every 10 – 15 min, such that a stable fluidized bed height of 0, 10, 20, 30, 35, 40 cm, and with larger additional heights above the inlet, was established during each experiment. At the start of each experiment, an initially measured pH of 10.0 was achieved, representing the conditions at the bottom of a full-scale pellet reactor.

2.3. Pilot-scale fluidized bed reactor experiments

FBR experiments were carried out in a metal-coated column of 5 m height (Fig. 2) with a reactor diameter $D_r = 310$ mm. For each new CP-layer addition, one bucket of CP (Fig. 2a) was added to the column (Fig. 2b and c) every 10 – 20 min throughout continuous operation (see SI-IX for the exact weights of each used bucket) and, depending on the hydrodynamic process conditions, amounted to the addition of 150 – 250 mm of fluidized bed. The FBR was equipped with pressure sensors at the bottom (Fig. 2d) to monitor potential clogging. During each experiment, the pH was monitored by multiple pH electrodes, both near the bed and at the top of the reactor near the water outlet. In addition, the depth or the height of the fluidized bed was measured with an ultrasound bed height meter, which was placed in the middle of the column (Fig. 2c). Furthermore, the EC was measured near the top of the fluidized bed. The water discharge was monitored with an automatic control valve (i.e., ABB process automation system; see SI-II) and the NaOH dosing volume was monitored similarly to PFR.

During each experiment, four water samples were taken (Fig. 2f) for calcium measurements, serving as an additional verification method, and 'crystallite area percentage' analysis, using respectively a calcium-ion selective electrode (Ca-ISE, see SI-II and SI-X for calibration and concentration calculation methods) and scanning electron microscopy (SEM; SI-II). In total, 17 FBR experiments were conducted at systematically varied NaOH dosing conditions, linear superficial fluid velocity (v_s), d_p and T (Fig. 2h). After each FBR experiment, the CP in the column was extracted at the bottom and three CP samples were collected, representing the bottom, middle, and top part of the fluidized bed (Fig. 2g).

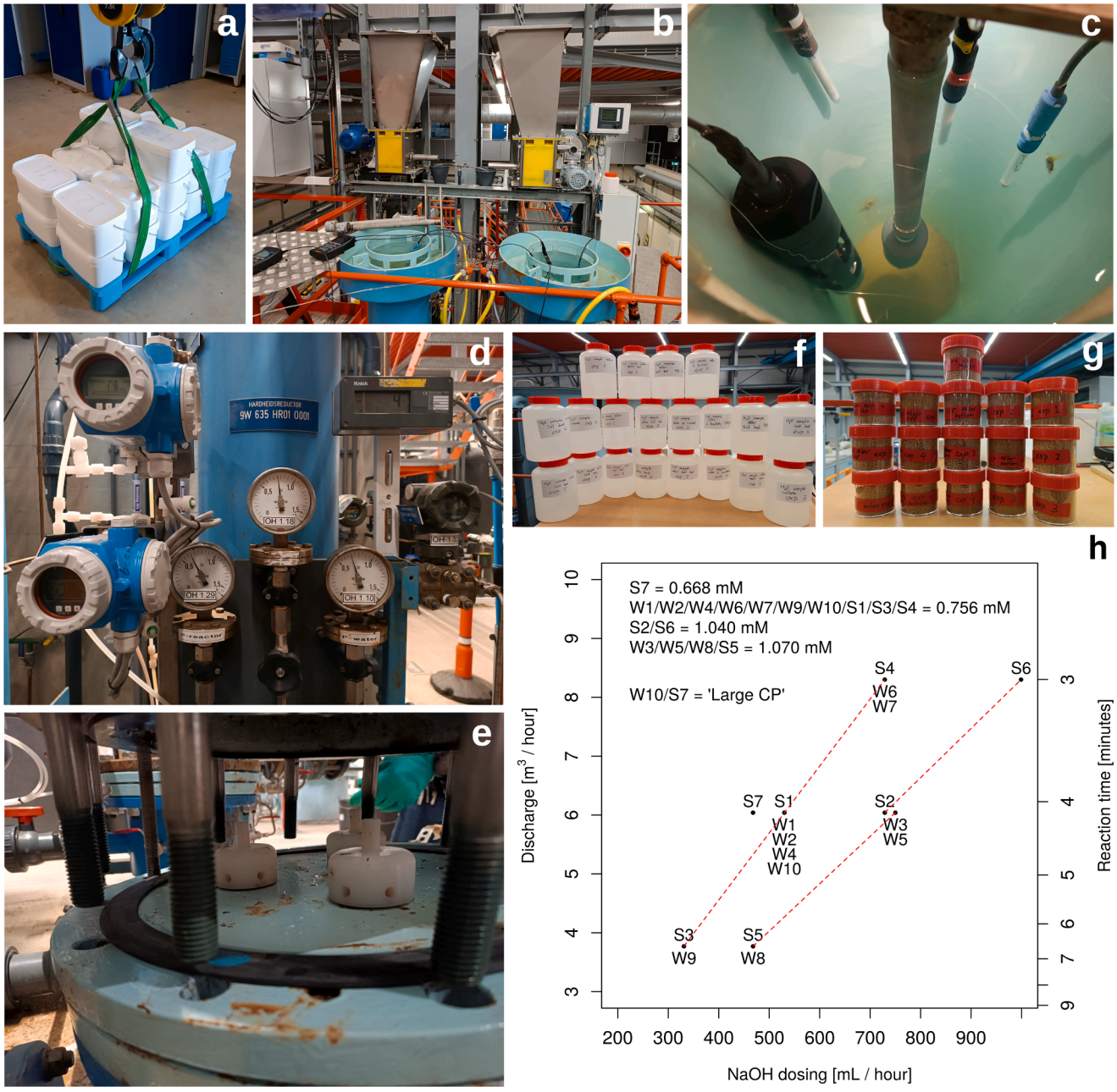

Fig. 2. Pilot-scale fluidized bed reactor (FBR) experimental set-up; calcite pellets distribution into buckets for experimental use (a), top-side view of the pilot-scale FBR (b), top-view into the FBR, showing the arrangement of monitoring sensors (c), bottom-view of the FBR, showing the pressure sensors for maintaining process control (d), internal view of the FBR at the bottom, displaying the water-NaOH dosing nozzles (e), extracted water samples (f), calcite pellet samples (g) and experimental conditions for each conducted FBR experiment (h). In (h), the red dashed lines indicate similar NaOH dosing concentrations.

These CP samples were compared to CP samples taken at the same height before the experiment was conducted (Section 3.5).

2.4. Data post-processing

Our choice to use pH measurements for calcium concentration was driven by their relatively higher degree of stability, lower susceptibility to Mg^{2+} interference, and suitability for continuous monitoring (Van Schagen (2009)), compared to Ca-ISE measurements, which showed higher variability and required more frequent recalibration (Section 3.4). The pH measurement data from CSTR, PFR, and FBR experiments were recalculated, under the assumption of a closed atmosphere (SI-XI), into calcium concentration and activity to improve the overall data quality. Furthermore, the kinetic calcium removal rates (r) and associated mass transfer coefficients (K_c) were determined for the CSTR experiments (SI-XII) and the derived K_c-values were compared with modeled values. The CP data analyses were conducted on samples of 3 g and the crystallite area percentage of each sample was derived from a filter area of 0.25–1 cm^2 and a 1 dm^2 image analysis area. A more detailed handling of the data can be found in SI-XII.

2.5. Model modifications for application across various reactor types

The total calcium removal rate (J_p) can be defined in the following conceptual way:

$$J_p = f\left(\begin{matrix}\text{particle}\\ \text{properties}\end{matrix}, \begin{matrix}\text{fluid}\\ \text{properties}\end{matrix}, \begin{matrix}\text{water matrix}\\ \text{properties}\end{matrix}, \begin{matrix}\text{reactor}\\ \text{properties}\end{matrix}\right) \quad (2)$$

where particle and fluid properties act as the (multiphase) system dynamics occurring in the different types of reactor, impacting the pathway between influent and effluent total calcium concentration (Ca_{tot}). Water matrix properties, such as softening chemical dosing, inhibitory effects, and impact of upstream processes, determine the (kinetic equilibrium) position of effluent Ca_{tot} conditions in the system. The reactor properties allocate the mixing type and efficiency, as well as the reactor properties and dimensions, thereby impacting the fluid-particle interaction and flow dynamics. Ultimately, the reactor properties in Eq. (2) impact the (prediction) accuracy of J_p and degree of homogeneity within the system.

While Seepma et al. (2025) proposed a new relationship for calcium removal (see SI-V), it predicts J_p without considering water matrix properties, such as the solution stoichiometry of the lattice ions, the presence of inhibitors, and effects of plant-wide drinking water treatment, which can significantly reduce J_p. Most notably though, their model does not take into account the reactor properties, such as the mixing dynamics of softening chemicals, influent hard water and seeding material. Therefore, to identify the level of impact of water matrix and reactor properties on calcium removal, Seepma et al. (2025)'s model was modified specifically for comparing our experimental calcium removal data with precipitation predictions across the different reactor types. In summary, for CSTR, the model was modified in terms of Reynolds number calculation (flow dynamics), leading to a different definition for Sherwood number (mass transfer) and ultimately impacts J_p. A more detailed discussion on the model modification is found in SI-V.

3. Results and discussion

In Sections 3.1 and 3.2, we discuss key experimental and model findings from CSTR experiments, focusing on the impact of varying T and SSA_W. Section 3.3 presents our PFR experimental findings, highlighting the impact of d_p, T, SI_{cal}, and upstream processes (i.e., ozonation), and compares these with CSTR results to elucidate the impact of mixing dynamics. Section 3.4 covers the FBR experimental work, where we varied T, d_p, v_s and SI_{cal}. Sections 3.5 and 3.6 discuss insights from the particle analysis of CP and $CaCO_3$ fines, respectively. In Section 3.7, we provide an integral qualitative impact assessment, critically examining the pivotal role of mixing dynamics in calcium removal across different softening experiments and evaluating the level of impact of the various studied physicochemical parameters. Finally, Section 3.8 provides the academic and societal implications of this study.

3.1. Effect of temperature and seeding material in CSTR experiments

The pH of the solution within the CSTR decreased with reaction time (t_r) at all three temperatures (i.e., $T = 5$, 20 and 40 °C) upon the onset of the $CaCO_3$ formation reaction (Fig. 3a–c). Similarly, the Ca_{tot} and Ω_{cal} decreased with t_r (Fig. 3d–i). The total calcium removal rate ($\Delta Ca_{tot}/\Delta t_r$) versus Ω_{cal} is shown in Fig. 3j–l. The different colours represent different m_s (Table 1). We show the results for the first 240 s, because it corresponds to the typical reaction time of influent hard water with CP in pellet-water softening treatment, where it generally ranges between 2.25 – 4.5 min.

We observed four main trends in the $CaCO_3$ reaction kinetics in the CSTR results. Foremost, more $CaCO_3$ powder led to faster crystallization reaction kinetics. The effect of m_s, determining the SSA (Table 1), on the crystallization kinetics is well-known and has been described thoroughly (Wiechers et al., 1975; Van Schagen et al., 2008; Kramer, 2021; Seepma et al., 2025). Secondly, we observed a significantly larger variance, up to 50 % (Fig. 3e), in the kinetics of experiments performed without added $CaCO_3$ powder (unseeded) and in the experiment with 1 g/L of added $CaCO_3$. This variance is likely attributed to the dominance of primary homogeneous nucleation at these conditions, coupled with increased uncertainty in SSA_W at low m_s. According to Equation S8 in SI-V, adjusted for CSTR applications, homogeneous nucleation accounts for $>$ 65 % of the total calcium removal at $m_s = 0$ g/L, and between 1 – 2 % at $m_s = 1$ g/L, regardless of T. In contrast, heterogeneous crystallization is the prevailing mechanism in seeded experiments with $m_s > 1$ g/L. The slower reaction kinetics observed at 0 g/L seed can be attributed to the higher kinetic energy barrier, as nucleation is more reaction-controlled compared to crystallization (Mullin, 2001). The uncertainty in the already low SSA_W at low m_s is exacerbated by the polydisperse and non-spherical nature of the $CaCO_3$ seed particles, as well as by the higher sensitivity to particle distribution inhomogeneity in the CSTR. Thirdly, we observed that, at $T = 5$ °C compared to $T > 5$ °C, the reaction proceeded much slower, where $m_s = 5$ g/L is not enough to reach the thermodynamic equilibrium in 240 s at $T = 5$ °C, while it does for $T > 5$ °C (Fig. 3d versus 3e and f). The observed temperature-dependent $CaCO_3$ precipitation kinetics is in line with earlier work (Gilmour et al., 1977; Østvold and Randhol, 2001; Carino et al., 2017 and references therein). Lastly, at $T = 40$ °C, we observed that thermodynamic equilibrium with respect to calcite was not reached within 240 s in any experiment. This observation may result from the more kinetically favourable conditions for aragonite formation at these elevated temperatures (Wray and Daniels, 1957; Ogino et al., 1987; Ma et al., 2010), before transforming into more (thermodynamically) stable calcite. This effect is evident in the pH and Ca_{tot} data deviating further from the calcite equilibrium line, as aragonite has a higher solubility product compared to calcite (Fig. 3c and f). In addition, the slower precipitation rate of aragonite compared to calcite at lower supersaturation (Burton and Walter, 1987) and the slightly higher degree of CO_2 degassing at elevated temperatures may have contributed to this observation.

Fig. 3j–l shows that the precipitation rate has a maximum value at the start of each experiment when the supersaturation degree is high (i.e., $\Omega_{cal} > 100$), and the rate decreases over time when Ω_{cal} is smaller. In addition, at $m_s \leq 5$ g/L and $T \geq 20$ °C, we observed that calcium precipitation rate is almost linear with Ω_{cal} until equilibrium, while at $m_s >$ 5 g/L, it can be approached as a bi-linear rate with a fast (r_{high}) and slow (r_{low}) rate. The critical point where the 'high' rate changes into a 'slow' rate is dependent on m_s and is located at increasingly lower Ω_{cal} with decreasing m_s (Fig. 3j–l). The high (r_{high}) and low (r_{low}) rates were

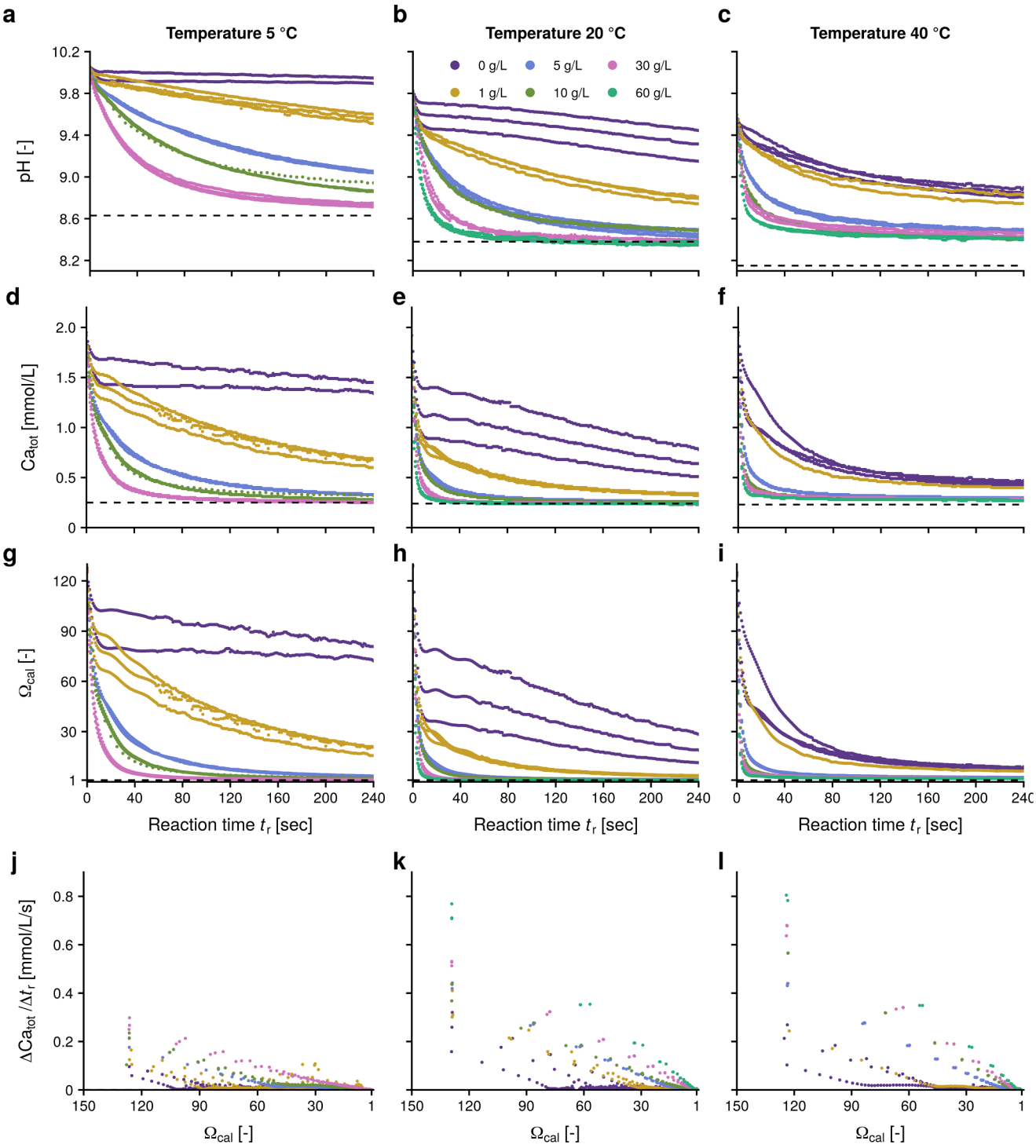

Fig. 3. CSTR experimental results at different temperature (column) and varying total seed mass (colour). The top row shows the pH measurement data (a-c), the second row the total calcium removal with time (d-f), the third row the decrease in supersaturation degree (Ω_{cal}) with time (g-i) and the bottom row the calcium removal rate with supersaturation degree (j-l).

subsequently translated to mass transfer coefficients (Section 2.4) and the numerically averaged values are shown in Table 2. The FBR model shows that K_c ranges roughly between $10^{-4} - 10^{-6}$ m s^{-1} (i.e., Fig. S23c and e in Seepma et al. (2025)). However, the calculated K_c-values from the CSTR experiments are consistently larger. Continuous agitation in a CSTR ensures that reactants are consistently brought into contact with the particles, leading to improved mass transfer rates (Levenspiel, 1999; Towler and Sinnott, 2021). Table 2 also shows that r_{low} is more influenced by SSA_W compared to r_{high}, and is especially pronounced at $T = 5$ °C. This translates also to the calculated K_c-values, where, for example, a five-fold increase in m_s did not lead to a five-fold decrease in K_c. In other words, at conditions far from equilibrium, mass transfer is driven by the concentration gradient, while at conditions near equilibrium, it is driven by surface area (Levenspiel, 1999).

Table 2
Average calculated kinetic calcium removal rates (r) from the measured CSTR data in Fig. 3 and calculated mass transfer crystallization rate coefficients (K_c).

m_s	$T = 5$ °C				$T = 20$ °C				$T = 40$ °C			
	r_{high}	r_{low}	$K_{c,\ high}$	$K_{c,\ low}$	r_{high}	r_{low}	$K_{c,\ high}$	$K_{c,\ low}$	r_{high}	r_{low}	$K_{c,\ high}$	$K_{c,\ low}$
[g]	[mol m^{-3} m^{-1}]		[m s^{-1}]		[mol m^{-3} m^{-1}]		[m s^{-1}]		[mol m^{-3} m^{-1}]		[m s^{-1}]	
0	2.10	0.140	9.45	0.630	3.17	0.340	15.3	1.64	2.70	0.240	15.1	1.34
1	2.63	0.170	0.118	0.00765	3.37	0.353	0.163	0.0170	3.05	0.340	0.171	0.0191
5	2.50	0.485	0.0225	0.00436	3.77	1.83	0.0363	0.0176	3.87	1.43	0.0433	0.0160
10	2.70	0.705	0.0121	0.00316	3.35	2.10	0.0161	0.0101	4.80	1.20	0.0268	0.00670
30	2.50	1.47	0.00371	0.00218	4.17	3.30	0.00663	0.00525	5.57	0.880	0.0103	0.00163
60	NA	NA	NA	NA	5.80	5.03	0.00456	0.00395	6.65	0.755	0.00607	0.000689

3.2. CSTR calcium removal measurement calculations versus model predictions

With the model adjustments, proposed in SI-V, the calculated SI_{cal}-values, based on pH measurement data of the solution, were used to obtain model predictions for the calcium removal with reaction time. The predictions were compared with the calcium removal rate derived from the measurements (Fig. 4). Note that $\{Ca^{2+}\}$ is shown rather than Ca_{tot}, because Equation S8 in SI-V is based on free calcium activity, that most experiments were done in triplicate and that Fig. 4a–c illustrate the comparison at varying temperature. Fig. 4a–c shows that at low SSA_W (i.e., at $m_s = 0 – 1$ g/L), the model underestimates the calcium removal rate by up to 30 %. In contrast, at high SSA_W (i.e., at $m_s = 30 – 60$ g/L), the model significantly overestimates the calcium removal rate by up to 100 %. This applies across all three temperature categories. Secondly, we observed that, in all cases, the initial decrease in $\{Ca^{2+}\}$ was much larger in the measurements compared to the prediction.

The large disparities between the measurement- and model-derived calcium removal are explained by hydraulic system dynamics, different reactor properties in CSTR compared to FBR, and environmental properties, which were not considered in the model. The underestimation at low SSA_W originates from (1) an underestimation of SSA_W, because it increases during the reaction time due to the formation of newly formed particles creating new nucleation sites for calcium removal, (2) point saturation at the beginning of the experiment due to NaOH addition by pipetting, leading to a steeper initial decrease compared to the model prediction and (3) the wall effect, which creates additional surface for faster calcium crystallization than is accounted for, and was evidenced by the need to clean the CSTR (with HCl acid) between experiments. The overestimation at high SSA_W originates from (1) more transport-limited conditions, instead of reaction-limited conditions, due to an increased local depletion of calcium near the particles, which likely occurred faster than the bulk mixing of the solutions (Kockmann, 2008), (2) a more pronounced inhomogeneous distribution of particles, with more particles residing in dead mixing zones within the reactor (Hurtado et al., 2015), which effectively reduces the available SSA_W, (3) the lack of metastable-zone conditions in the model (Elfil and Roques, 2004; Sobhan, 2019), (4) increased aggregation conditions due to increased particle collision frequencies (Smoluchowski, 1916), leading to a further decrease of effective SSA_W (Kramer et al., 2020) and (5) inhibition by other ions present in the water matrix, especially TOC and Mg (SI-XIV). Finally, the highly turbulent flow conditions in the CSTR likely impact the pH measurements in a more negative way (McMillan and Cameron, 2004), as it will have more challenges to provide equilibrated values compared to PFR and FBR. Ultimately, the mixing process and turbulent flow conditions impact the fluid-particle interactions differently in CSTR compared to FBR and lead to increased inaccurate model predictions.

3.3. Influence of key process parameters on softening efficiency in CSTR and PFR experiments

PFR experiments were conducted alongside CSTR experiments. Despite similar conditions of T and NaOH dosing concentrations in both CSTR and PFR experiments, d_p and v_s varied significantly (i.e., $d_p = 26.3$ μm and $v_s \sim 380$ m/h in CSTR and respectively ~ 1.1 mm and 80 m/h in PFR). The effect of NaOH dosing, temperature, the type of seeding material, and the influent water matrix are discussed in the following subsections followed by a comparison of the reaction kinetics in CSTR and PFR.

3.3.1. Effect of NaOH dosing

The effect of NaOH dosing shows that an optimum is found at 2.0 mmol/L for both raw and ozonated WPK water for this PFR column and its water residence time (τ_r) of about 40 s for $v_s = 80$ m/h. This is observed by the green-coloured lines reaching near-equilibrium at maximum fluidized bed height conditions (Fig. 5a). At NaOH dosing concentrations below 2.0 mmol/L, the Ca_{tot} concentrations at maximum fluidized bed height conditions progressively deviated from equilibrium. Notably, at NaOH = 2.5 mmol/L, near-equilibrium conditions were reached at $t_r \sim 20$ s. However, operational challenges arose, including clogging in the PFR set-up, which limited data collection beyond this point.

3.3.2. Impact of prior ozonation on softening performance

Non-ozonated water is softened more efficiently than ozonated water, with up to 10 % more calcium removal at NaOH = 1.5 mmol/L under identical process conditions (Fig. 5a). This difference is reflected in the smaller distance to the equilibrium line for non-ozonated water across all NaOH dosing conditions. One explanation is the larger capacity to inhibit $CaCO_3$ precipitation by an increased number of small organic molecules (Meldrum and Cölfen, 2008), which are more abundant in ozonated water. Ozonation enhances the formation of more easily degradable organic material such as assimilable organic carbon (AOC) and interacts strongly with the seeding material by promoting biological activity that consumes AOC (Hammes et al., 2011). This effect is particularly relevant for WPK water, which contains relatively high concentrations of TOC, attributed to the natural presence of humic acids (SI-III). Additional experiments using synthetic water with varying concentrations of TOC showed that a longer t_r is required to reach equilibrium (Fig. S9 in SI-XIV) and supports the observation of increased inhibition by TOC in ozonated WPK water.

3.3.3. Effect of temperature effect and seeding material on reaction kinetics in PFR

The PFR experiments at $T = 40$ °C approached equilibrium initially at a faster rate compared to $T = 10$ and 20 °C (Fig. 5b), which is consistent with our CSTR findings (Fig. 3). However, at fully fluidized bed conditions, the experiments at $T = 40$ °C approached equilibrium more closely than at lower temperatures, contrasting the CSTR results. One possible explanation is the reduced CO_2 degassing during operation at 40 °C, which reduces the systematic error for the pH-derived Ca_{tot} in PFR compared to CSTR. In addition, despite the presence of a static mixer at the inlet, the PFR inherently exhibits local supersaturation gradients in both the axial and radial directions. These gradients promote localized precipitation, where supersaturated water precipitates

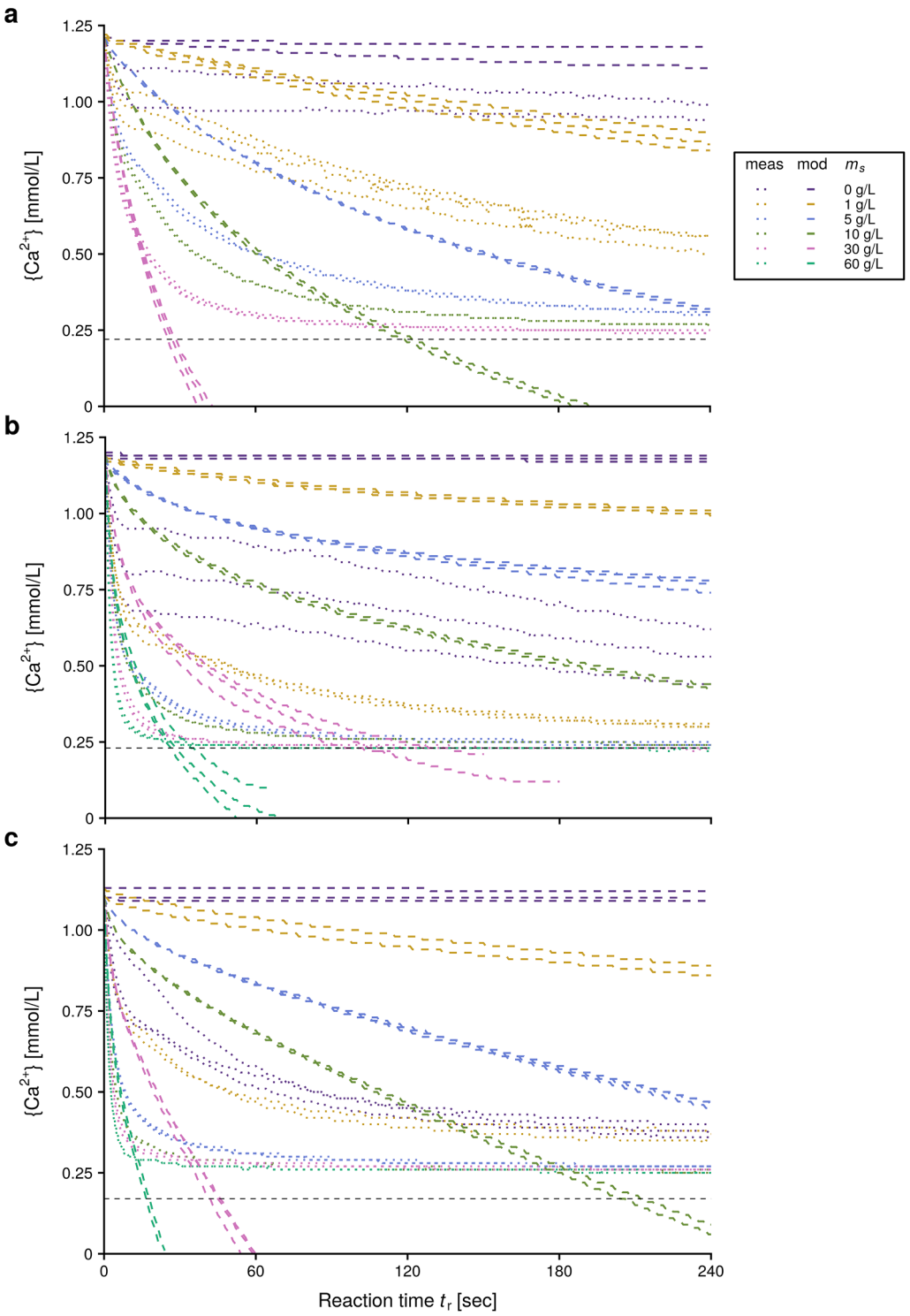

Fig. 4. CSTR calculated {Ca^{2+}} based on measurement pH data versus model predictions for $T = 5$ °C (a), 20 °C (b) and 40 °C (c). The horizontal black dashed lines show the equilibrium activity lines. Note that in (b) some data were omitted for clarity and that the figure containing all data is found in SI-XIII.

rapidly in certain zones before mixing with less supersaturated water downstream, following an internal bypass effect within the reactor. Following from Fig. 5b, the temperature-dependent trends were independent of particle shape and size, with both larger, rounded CP particles and smaller, angular crushed calcite (CC) showing similar behaviour.

3.3.4. Comparison of reaction kinetics in CSTR and PFR

A comparison of PFR and CSTR experiments (Fig. 5c) shows that CSTR experiments exhibited faster reaction kinetics, reaching near-equilibrium conditions more rapidly. This difference is primarily attributed to differences in reactor design and spatial scales. In PFR setups, the conversion yield is typically higher than in CSTR under identical process conditions (e.g., T, τ_r, SSA_W) for equal volumes of softened water (Levenspiel, 1999). However, our calculations indicate that, with some assumptions, ν_s in the CSTR was significantly higher, averaging 4 to 5 times that of the PFR (SI-V). In the CSTR, the entire volume (1 L) is softened simultaneously, whereas the same volume is processed in the

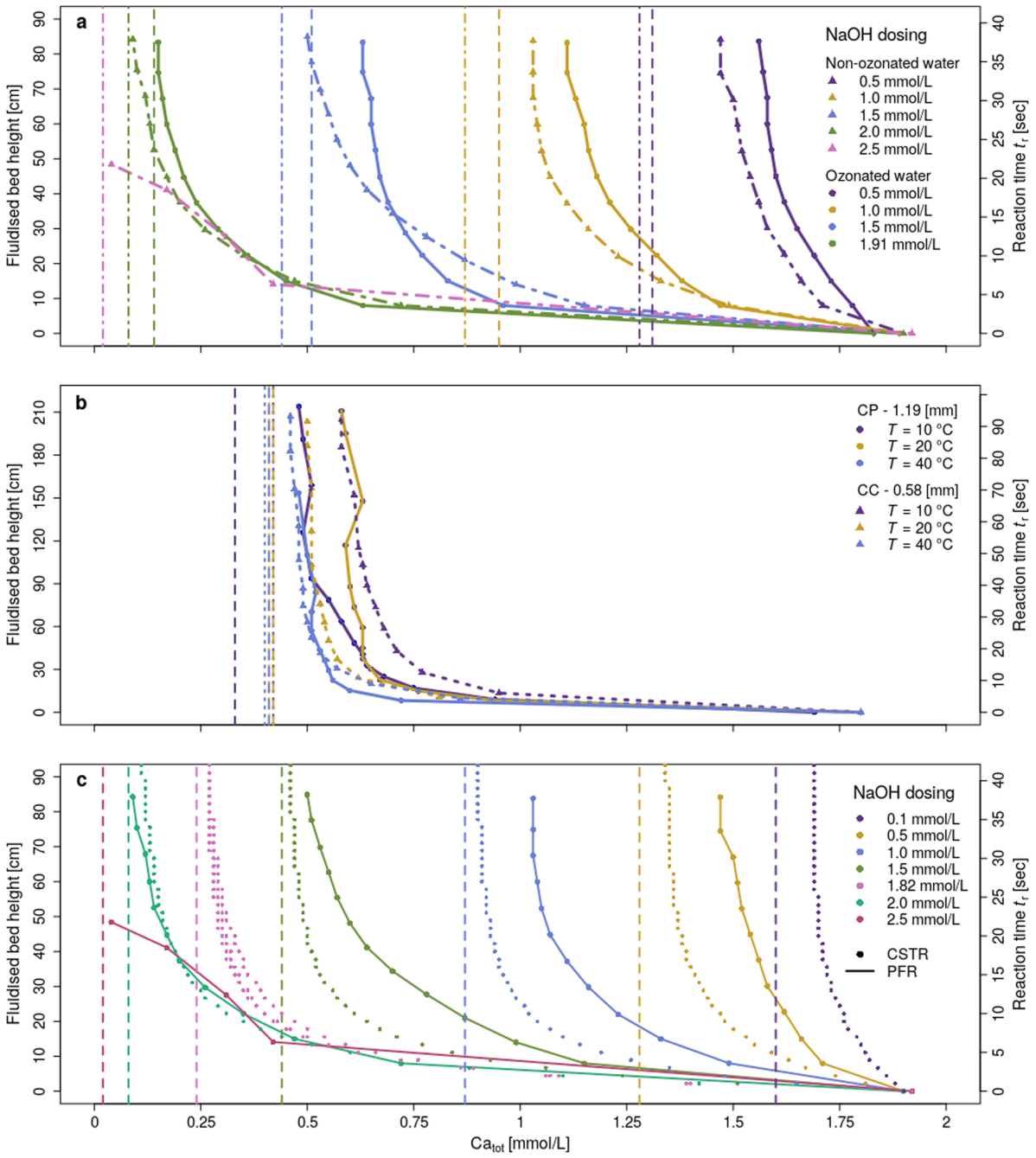

Fig. 5. Total calcium removal (Ca_{tot}) with fluidized bed height (FBR) and equivalent reaction time (CSTR) for non-ozonated versus ozonated water at varying NaOH dosing conditions at $T = 20$ °C (a), for well-rounded calcite pellets versus angular crushed calcite (CC) at varying temperatures (b) and for CSTR versus FBR at varying NaOH dosing conditions at $T = 20$ °C (c). The vertical dashed lines and dashed-dotted lines show the equilibrium conditions for the corresponding experiment(s).

PFR every ~8.6 s at $v_s = 80$ m/h. The higher v_s in the CSTR promotes faster mass transfer, contributing to the observed differences in reaction kinetics. In addition, the higher v_s in the CSTR leads to increased turbulent flow conditions, favouring reaction-controlled mass transfer conditions. Contrastingly, the PFR setup operates in the transitional flow regime (based on Re and Sh calculations; i.e., Figs. S8a and S23b in Seepma et al. (2025)), where transport-controlled mass transfer may be more pronounced. An exception to this trend was observed at NaOH = 2.0 mmol/L, where the difference in reaction kinetics between CSTR and PFR experiments was negligible. In this case, transport limitations were likely overcome due to the high NaOH dosing concentration.

3.4. Full-scale FBR experiments: measurement-derived calcium removal versus model predictions

The measured calcium carbonate precipitation rate in the lower sections of the full-scale FBR was five to ten times higher than the model predictions (Fig. 6a; showing experiments #S2 and #S7 that respectively have the worst and best $CaCO_3$ removal model predictions compared to the experimental data) and was consistent across the entire range of process conditions tested (i.e., $v_s = 50 - 110$ m/h, $d_p = 1.0 - 1.9$ mm, $T = 5 - 21$ °C, initial $SI_{cal} = 1.73 - 1.92$) in the FBR experiments (Fig. 2h and SI-XV for the results). The deviation is explained by model assumptions on homogeneous and instantaneous mixing of hard water, caustic soda and seeding material, while experimental observations

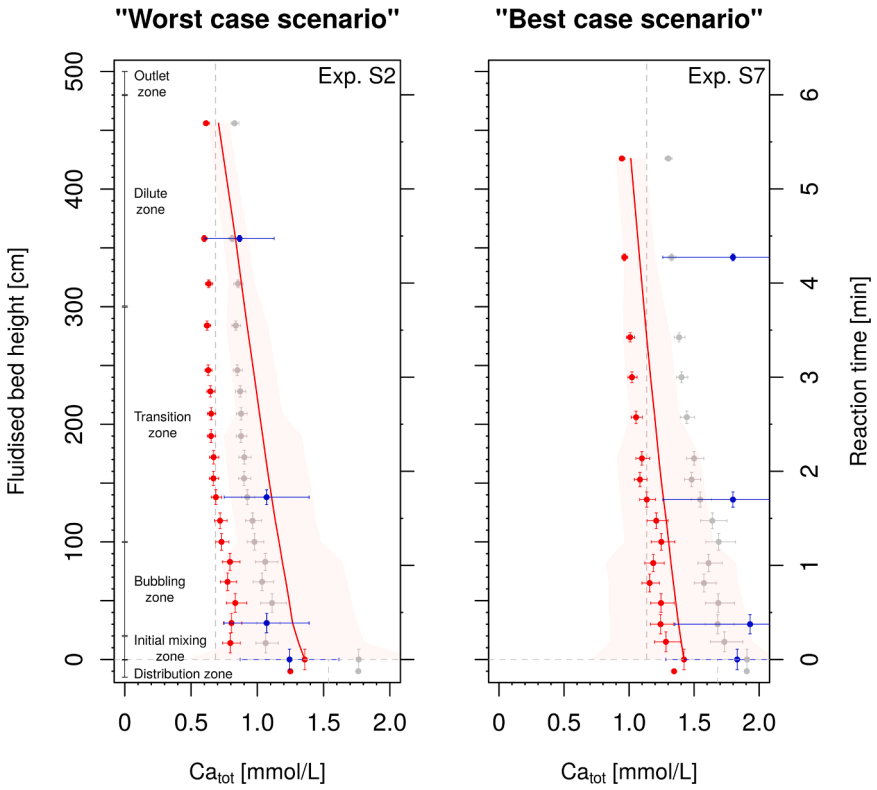

Fig. 6. Fluidized bed height versus total calcium for the worst (#S2) and best (#S7) case scenarios with regards to the match between derived measured Ca conditions and model predictions. The pH-derived total calcium concentrations, total calcium activity and total calcium concentrations derived from Ca-ISE measurements (see SI-X for calibration and calculation methods) are shown in respectively grey, red and blue. The red solid lines represent the model predictions of Ca removal (as $CaCO_3$) using the model of Seepma et al. (2025) and the red-shaded area as its confidence interval. More details are found in SI-XV.

suggest that ideal mixing was not fully achieved in any case (Fig. 6a). Under the assumption of ideal mixing, calculations estimated an initial $\Omega_{cal} = 1.7 - 2.0$. However, based on the difference between measured and modeled $\{Ca^{2+}\}$ at the reactor bottom, the initial Ω_{cal} is more likely between 2.3 and 2.5, and overcomes the observed difference in Ca_{tot} at the reactor bottom. Midway and at the top of the reactor, the model overpredicted precipitation rates by approximately 2 to 3 times. This overprediction is likely explained by inhibitory effects (see SI-XIV for results and discussion on experiments conducted with inhibitors), due to the presence of TOC and magnesium. While PO_4 is known to inhibit $CaCO_3$ formation (Lin and Singer, 2005b) and SO_4 slightly promotes it (Zhu et al., 2022; Fig. S7 in SI-XIV), these ions are present only in minor fractions (Tables S3 and SI-III). Furthermore, the r_{aq} increases from approximately 3 up to 40 toward the top of the reactor (SI-IX), likely slowing down $CaCO_3$ formation kinetics negligibly within this range of r_{aq} (e.g., Wolthers et al., 2012; Seepma et al., 2021). Other factors contributing to the model's overestimation at the top include: (1) the assumption of a linear decrease in CP diameter with fluidized bed height, which was based on only three CP samples per experiment, despite Kramer et al. (2021) demonstrating that this linearity is inaccurate; (2) the use of an average v_s and T for the axial locations of pH measurements; and (3) variations in maintenance of the dosing nozzles and the FBR column during experiments.

In summary, although slight nuances were found between the FBR experiments (SI-XV), the range of process conditions used in FBR water softening do not seem broad enough to reveal significant impacts of process conditions on fluid characteristics beyond the bottom sections of the reactor. Yet, comparisons between measured and modeled $CaCO_3$ removal rates at varying process conditions highlight the significant impact of factors such as mixing dynamics, uncertainties related to axial uniformity and the accuracy of pH measurement devices on process performance. Although fluid characterization showed that T (i.e., winter versus summer experiments) had a moderate impact on the $CaCO_3$ removal rate, it remains challenging to conduct a qualitative impact assessment based on fluid characteristics alone. Therefore, particle characterization of CP (Section 3.5) and $CaCO_3$ fines in water samples (Section 3.6) was carried out to provide additional insight.

3.5. CP sample analysis

Particle size, shape, and the resulting calculated specific surface area and specific space velocity (SI-V) did not change significantly during the experiments (see SI-XVI, SI-XVII for raw and processed data and images, and SI-XVIII for processing methods). Still some systematic changes were observed, which are discussed in SI-XVI.

3.6. Fines formation via homogeneous nucleation

In all FBR experiments, the area percentage of $CaCO_3$ fines showed an optimum at a fluidized bed height (h_r) < 1.50 m, and decreased significantly to < 20 % at $1.50 < h_r < 4.50$ m (Fig. 7, see also SI-XIX and SI-XX for detailed methods and image results). Seasonal variations were observed, with summer experiments exhibiting a higher proportion of $CaCO_3$ fines at the top of the FBR compared to winter experiments (i.e., 7.4 % ± 4.6 % versus 2.8 % ± 1.7 %). This trend indicates a larger carry-over of fines to downstream treatment processes and a lower conversion yield during summer. This observation aligns with the retrograde solubility behaviour of calcite, where higher temperatures in summer promote greater fines formation by nucleation relative to the increase in crystallization (SI-XXI). Furthermore, during the end of winter/early spring, the TOC concentration in WPK water is largest, while at the end of summer/start of fall, it is generally at its lowest concentration. Therefore, it is plausible that more TOC is removed by incorporation into CP and in $CaCO_3$ fines, which may explain the lower concentration

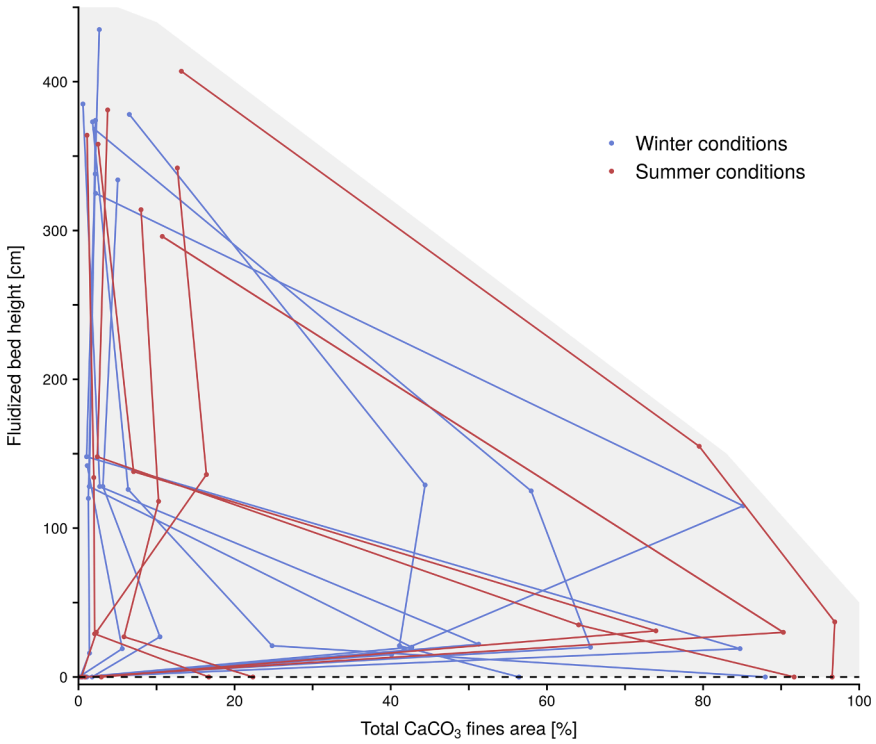

Fig. 7. Fluidized bed height versus total $CaCO_3$ fines area [%] based on experimental data (SI-XIX and SI-XX). The black dashed line shows $h_r = 0$ (no pellet bed). A more detailed version of this figure, distinguishing between individual experiments, is available in SI-XIII.

during late summer in the aqueous phase of the softening effluent (SI-XXI). The experiments conducted with the largest average CP diameter (i.e., $d_p = 1.8 – 1.9$ mm in #W10 and #S7) exhibited the second-highest $CaCO_3$ fines area percentages at the top of the FBR when grouped by season. This suggests that d_p plays a significant role in recrystallization efficiency during pellet softening (Seepma et al., 2025).

3.7. Classification of investigated physicochemical parameters

Our experimental findings allow us to qualitatively assess the relative importance of different drivers (i.e., investigated physicochemical parameters) for calcium removal during softening. The impact of these parameters on the $CaCO_3$ removal rate (J_p), indicative for the softening performance, is reflected by five key reactor performance indicators (KPIs; Seepma et al., 2025), and each parameter may impact one or more KPIs. This is summarized in Table 3. The most critical parameters for J_p in CSTR are v_s, the mixing time necessary for achieving an instantaneous and homogeneous particle-fluid system (t_m), and the NaOH dosing. In PFR and FBR, other factors such as SSA_W and residence time τ_r contribute to a larger degree as well, besides v_s, t_m and NaOH dosing. While improving factors with lower influence may enhance the softening performance, prioritizing the high and moderate influencing factors is recommended. Our findings, summarized in Table 3, may aid in future softening reactor design and operations as well as improving current softening operations and may lead to reduced operational costs.

3.8. Implications

The new insights, summarized in Table 3, have broader implications for the field of water treatment and reactor engineering. By understanding the hierarchical importance of various physicochemical parameters, engineers are able to design more efficient, sustainable and future-proof reactors, tailored to specific environmental conditions and treatment goals. Furthermore, the qualitative impact assessment method presented here can be adapted for evaluating other complex (multiphase flow) systems, where numerous interacting parameters influence performance outcomes. Future research could expand on these findings by exploring the interplay between these factors in different reactor configurations and scaling up experiments to real-world industrial-scale applications.

The practical application value of our integral impact assessment is demonstrated in the site-specific case of WPK. Combined with scenario modelling (Seepma et al. (2025)), the assessment identified recrystallization efficiency as the key limiting factor in the softening process performance. Enhancing this KPI offers the greatest potential for improvement. Our cost-benefit analysis (SI-XXII) supports the business case for increasing the pellet-softening reactor height to 10 m, thereby extending the water residence and provide more flexibility to meet future water demands (Kramer, 2021). With an estimated return on investment of approximately 7 years, this modification aligns with the expected operational lifespan of 15–20 years, ensuring long-term viability and operational sustainability.

4. Conclusions

Our multi-scale experimental findings have elucidated the importance and impact level of various particle, fluid, reactor, and water matrix properties on calcium (as $CaCO_3$) removal during water softening practices. Our key findings from the integral qualitative impact assessment are:

- The linear superficial velocity (v_s), the mixing time to achieve a homogeneous particle-fluid system (t_m) and NaOH dosing are the high influencing factors driving the softening process in continuous-stirred tank reactor conditions.
- The specific surface area per water volume (SSA_W) and residence time (τ_r) are more significant in plug-flow reactor and fluidized bed reactor conditions, besides v_s, t_m and NaOH dosing.
- Application of Seepma et al. (2025)'s model to our experimental findings shows two major shortcomings:

Table 3
Integral qualitative impact assessment on physicochemical parameters affecting key reactor performance indicators, driving the softening process' performance. d_p is the average particle diameter, χ_s the particle shape factor, SSA_W the specific surface area per water volume, T the temperature, v_s the linear superficial fluid velocity, t_m the mixing time to obtain a homogeneous particle-fluid system, SSV the specific space velocity, J_c / J_p the ratio between crystallization and total precipitation rate, Sh the Sherwood number indicating the convective mass transfer compared to diffusional mass transfer, $CCPP_{rel}$ the calcium carbonate precipitation potential relative to the initial concentrations and f_r the recrystallization factor and where NI stands for negligible influence, LI for low influence, MI for moderate influence, HI for high influence and NA for not available.

Category	Varied in experiments	Impact on KPI	Level of influence on performance			Notes
			CSTR	PFR	FBR	
Particle properties	d_p	SSV, J_c / J_p, Sh	NI	LI	LI	In PFR and FBR low influence as long as $d_p > 0.8$ mm and $T \geq 5$ °C
	χ_s	SSV, J_c / J_p, Sh	NI	LI	NI	PFR slightly more significant due to lower τ_r compared to FBR.
	SSA_W	SSV, J_c / J_p, f_r	LI	MI	MI	When SSA_W conditions in CSTR resemble those at standard pellet softening conditions, t_r is sufficient to obtain similar degree of softening. In PFR and FBR more important due to larger t_m.
Fluid properties	T	SSV, $CCPP_{rel}$, J_c / J_p, Sh	MI	MI	MI	Temperature influences $CaCO_3$ system equilibria at similar degree in CSTR, PFR and FBR. Sh deviates about 15% through the seasons in CSTR and about 50% in PFR and FBR.
	v_s	SSV, J_c / J_p, Sh, f_r	HI	MI	MI	In CSTR, v_s is the main driver for Sh. In PFR and FBR, it impacts Sh relatively less at operating conditions, but f_r may be impacted by as much as 70%, besides Sh.
Reactor properties	t_m	J_c / J_p, Sh	HI	HI	HI	In CSTR, PFR and FBR, t_m is the main driver for the model offset predictions. Larger t_m increases nucleation and lowers Sh.
	τ_r	f_r	LI	HI	HI	In CSTR, it plays a minor role as long as $SSA_W > 1800$ m^2 m^{-3}. In PFR and FBR it is most crucial and depends on reactor dimensions besides v_s.
Water matrix properties	NaOH dosing	$CCPP_{rel}$, J_c / J_p	HI	HI	HI	NaOH dosing has a relatively small window for operating at high performance and is a trade-off between obtaining high $CCPP_{rel}$, while keeping J_c / J_p high as well, ensuring seeded crystallization.
	Inhibition	$CCPP_{rel}$, J_c / J_p	LI	MI	LI	When SSA_W conditions in CSTR resemble those at standard pellet softening conditions, TOC, Mg and SO_4 at regular concentration levels don't influence the total calcium removal when $t_r \geq 4$ min. In PFR, it has the largest influence due to transport-limited conditions.
	Ozonation	$CCPP_{rel}$, J_c / J_p	NA	MI	LI	Similar to inhibition, although for CSTR, the effect was not tested.

- The assumption of instantaneous and homogeneous mixing between softening chemicals, influent hard water, and seeding material, leading to inaccurate calcium removal predictions at reaction time < 10 s in CSTR or the bottom section in PFR and FBR.
- The model's applicability to reactor designs with highly turbulent conditions, such as continuous-stirred tank reactor conditions, is limited.

CRediT authorship contribution statement

Sergëj Y.M.H. Seepma: Writing – review & editing, Writing – original draft, Visualization, Validation, Methodology, Investigation, Formal analysis, Data curation. **Janou A. Koskamp:** Writing – review & editing, Software, Investigation, Formal analysis, Data curation. **Michel G. Colin:** Writing – review & editing, Supervision, Resources, Project administration, Funding acquisition, Conceptualization. **Eleftheria Chiou:** Writing – review & editing, Methodology, Investigation, Conceptualization. **Rubayat Sobhan:** Writing – review & editing, Methodology, Investigation, Conceptualization. **Tim F.J. Bögels:** Writing – review & editing, Methodology, Investigation, Conceptualization. **Tom Bastiaan:** Writing – review & editing, Methodology, Investigation, Conceptualization. **Hadi Zamanian:** Writing – review & editing, Investigation, Data curation. **Eric T. Baars:** Writing – review & editing, Supervision, Methodology. **Peter J. de Moel:** Writing – review & editing, Supervision, Software, Methodology. **Mariëtte Wolthers:** Writing – review & editing, Supervision, Resources, Project administration, Funding acquisition, Data curation, Conceptualization. **Onno J. I. Kramer:** Writing – review & editing, Supervision, Software, Resources, Project administration, Methodology, Data curation, Conceptualization.

Declaration of competing interest

The authors declare that they have no known competing financial interests or personal relationships that could have appeared to influence the work reported in this paper.

Acknowledgements

The authors thank F. te Pas, M. Heuver, M. Joosten, P. Wind, B. van der Sluijs for their contribution in the arrangement of materials and equipment in the Waternet Weesperkarspel pilot plant and L. Kors for the administrative arrangements of having access to the treatment plant facilities.

Funding

This work was supported by the European Research Council (ERC) under the European Union's Horizon 2020 Research and innovation programme (grant agreement no. 819588) to M.W., S.Y.M.H.S. and J.A. K.

Supplementary materials

Supplementary material associated with this article can be found, in the online version, at doi:10.1016/j.watres.2025.123647.

It contains details on the definition of process conditions ranges of values (I), standard operating procedure (II), composition of WPK influent water used during softening experiments (III), NaOH concentration measurement (IV), model adjustment equations for model application in CSTR conditions (V), particle size distribution of $CaCO_3$ powder used in CSTR (VI), pH measurement precision (VII), particle size distribution of $CaCO_3$ powder used in PFR (VIII), tabulated details on FBR experiments (IX), calibration and concentration calculation methods for Ca-ISE measurements (X), effect of atmospheric CO_2 in CSTR (XI), data post-processing (XII), alternative figures (XIII), inhibition effects (XIV), FBR experimental data on all 17 experiments (XV), calcite pellet analysis discussion and raw and post-processed data (XVI-XVIII), $CaCO_3$ fines raw and post-processed data (XIX+XX), temperature-dependent $CaCO_3$ fines productions (XXI) and feasibility analysis on proposed softening operations modification at WPK (XXII).

References

Barrios, R., Siebel, M., Van der Helm, A., Bosklopper, K., Gijzen, H., 2008. Environmental and financial life cycle impact assessment of drinking water production at Waternet. J. Clean. Prod. 16 (4), 471–476. https://doi.org/10.1016/j.jclepro.2006.07.052.

Burton, E.A., Walter, L.M., 1987. Relative precipitation rates of aragonite and Mg calcite from seawater: temperature or carbonate ion control? Geology 15 (2), 111–114. https://doi.org/10.1130/0091-7613(1987)15<111:RPROAA>2.0.CO;2.

Burton, F.L., Tchobanoglous, G., Tsuchihashi, R., Stensel, H.D., 2013. Wastewater engineering: Treatment and Resource Recovery, 5th ed. McGraw-Hill, New York, NY.

Carino, A., Testino, A., Andalibi, M.R., Pilger, F., Bowen, P., Ludwig, C., 2017. Thermodynamic-kinetic precipitation modeling. A case study: the amorphous calcium carbonate (ACC) precipitation pathway unravelled. Cryst. Grow. Des. 17 (4), 2006–2015. https://doi.org/10.1021/acs.cgd.7b00006.

Carman, P., 1937. Fluid flow through a granular bed. Trans. Inst. Chem. Eng. 15, 150–167. https://doi.org/10.1016/S0263-8762(97)80003-2.

Crittenden, J.C., Trussell, R.R., Hand, D.W., Howe, K.J., Tchobanoglous, G., 2012. MWH's Water treatment: Principles and Design, 3rd ed. John Wiley & Sons, New York, NY.

Eke, J., Yusef, A., Giwa, A., Sodiq, A., 2020. The global status of desalinization: an assessment of current desalinization technologies, plants and capacity. Desalinization 495, 114633. https://doi.org/10.1016/j.desal.2020.114633.

Elfil, H., Roques, H., 2004. Prediction of the metastable zone in the "$CaCO_3$-CO_2-H_2O" system. AlChE J. 50 (8), 1908–1916. https://doi.org/10.1002/aic.10160.

Gilmour, J.T., Shirk, K.S., Ferguson, J.A., Griffis, C.L., 1977. A kinetic study of the $CaCO_3$ precipitation reaction. Agric. Water Manag. 1 (3), 253–262. https://doi.org/10.1016/0378-3774(77)90004-x.

Hammes, F., Boon, N., Vital, M., Ross, P., Magic-Knezev, A., Dignum, M., 2011. Bacterial colonization of pellet softening reactors used during drinking water treatment. Appl. Environ. Microbiol. 77 (3), 1041–1048. https://doi.org/10.1128/AEM.02068-10.

Hofman, J.A.M.H., Kramer, O.J.I., Van der Hoek, J.P., Nederlof, M.M., Groenendijk, M., 2006. Twenty years of experience with central softening in The Netherlands, water quality, environmental benefits and costs. In: Presented at the International Symposium on Health Aspects of Calcium and Magnesium in Drinking Water. Washington, DC.

Hurtado, F.J., Kaiser, A.S., Zamora, B., 2015. Fluid dynamic analysis of a continuous stirred tank reactor for technical optimization of wastewater digestion. Water Res. 71, 282–293. https://doi.org/10.1016/j.watres.2014.11.053.

Kockmann, N., 2008. Transport Phenomena in Micro Process Engineering. Springer Science & Business Media, Berlin, Germany. https://doi.org/10.1007/978-3-540-74618-8.

Kozeny, J., 1927. Über kapillare Leitung des Wassers im Boden. *Sitzungsber.* Akad. Wiss. Wien 136 (2a), 271–306.

Kramer, O.J.I., De Moel, P.J., Padding, J.T., Baars, E.T., El Hasadi, Y.M., Boek, E.S., Van der Hoek, J.P., 2020. Accurate voidage prediction in fluidisation systems for full-scale drinking water pellet softening reactors using data driven models. J. Water Process Eng. 37, 101481. https://doi.org/10.1016/j.jwpe.2020.101481.

Kramer, O.J.I., Van Schaik, C., Hangelbroek, J.J., De Moel, P.J., Colin, M.G., Amsing, M., Boek, E.S., Breugem, W.P., Padding, J.T., Van der Hoek, J.P., 2021. A novel sensor measuring local voidage profile inside a fluidised bed reactor. J. Water Process Eng. 42, 102091. https://doi.org/10.1016/j.jwpe.2021.102091.

Kramer, O.J.I., 2021. Hydraulic Modelling of Liquid-Solid Fluidisation in Drinking Water Treatment processes. Doctoral Dissertation. Delft University of Technology, Department of Civil Engineering and Geosciences.

Levenspiel, O., 1999. Chemical Reaction Engineering, 3rd ed. John Wiley & Sons, New York, NY.

Lin, Y.P., Singer, P.C., 2005a. Effects of seed material and solution composition on calcite precipitation. Geochim. Cosmochim. Acta 69 (18), 4495–4504. https://doi.org/10.1016/j.gca.2005.06.002.

Lin, Y.P., Singer, P.C., 2005b. Inhibition of calcite crystal growth by polyphosphonates. Water Res. 39 (19), 4835–4843. https://doi.org/10.1016/j.watres.2005.10.003.

Ma, Y.F., Gao, Y.H., Feng, Q.L., 2010. Effects of pH and temperature on $CaCO_3$ crystallization in aqueous solution with water soluble matrix of pearls. J. Cryst. Grow. 312 (21), 3165–3170. https://doi.org/10.1016/j.jcrysgro.2010.07.053.

McMillan, G.K., Cameron, R.A., 2004. Advanced pH Measurement and Control, 3rd ed. The Instrumentation, Systems, and Automation Society, Durham, NC.

Meldrum, F.C., Cölfen, H., 2008. Controlling mineral morphologies and structures in biological and synthetic systems. Chem. Rev. 108 (11), 4332–4432. https://doi.org/10.1021/cr80022856.

Mitchell, P., 2008. Central heating, installation, Maintenance and Repair. Brailsford Press, Eachwick, UK.

Mons, M., Van Dijk, H., Gatel, D., Hesse, S., Hofman, J., Nguyen, M.L., Slaats, N., 2007. Drinking Water hardness: Reasons and Criteria For Softening and Conditioning of Drinking Water. Global Water Research Coalition, London, UK.

Mullin, J.W., 2001. Crystallization, 4th ed. Butterworth-Heinemann, Oxford, MA.

Nancollas, G.H., Reddy, M.M., 1971. The crystallization of calcium carbonate: II. Calcite growth mechanism. J. Colloid Interface Sci. 37 (4), 824–830. https://doi.org/10.1016/0021-9797(71)90363-8.

Nijssen, T.M.J., Kramer, O.J.I., De Moel, P.J., Rahman, J., Kroon, J.P., Berhanu, P., Boek, E.S., Buist, K.A., Van der Hoek, J.P., Padding, J.T., Kuipers, J.A.M., 2021. Experimental and numerical insights into heterogeneous liquid-solid behaviour in drinking water softening reactors. Chem. Eng. Sci.: X 11, 100100. https://doi.org/10.1016/j.cesx.2021.100100.

Nilsson, Ö., Sternbeck, J., 1999. A mechanistic model for calcite crystal growth using surface speciation. Geochem. Cosmochim. Acta 63 (2), 217–225. https://doi.org/10.1016/S0016-7037(99)00026-5.

Ogino, T., Suzuki, T., Sawada, K., 1987. The formation and transformation mechanism of calcium carbonate in water. Geochim. Cosmochim. Acta 51 (10), 2757–2767. https://doi.org/10.1016/0016-7037(87)90155-4.

Østvold, T., Randhol, P., 2001. Kinetics of $CaCO_3$ scale formation. The influence of temperature, supersaturation and ionic composition. In: Presented at International Symposium on Oilfield Scale. https://doi.org/10.2118/68302-MS. Aberdeen, UK.

Palmen, L.J., Schetters, M.J.A., Van der Hoek, J.P., Kramer, O.J.I., Kors, L.J., Hofs, B., Koppers, H., 2014. Circular Economy in Drinking Water treatment: Reuse of Grinded Pellets As Seeding Material in the Pellet-Softening Process. Presented at IWA World Water Congress and Exhibition, Lisbon, Portugal.

Reddy, M.M., Nancollas, G.H., 1971. The crystallization of calcium carbonate: I. Isotopic exchange and kinetics. J. Colloid Interface Sci. 36 (2), 166–172. https://doi.org/10.1016/0021-9797(71)90161-5.

Richardson, J.F., Zaki, W.N., 1954. The sedimentation of a suspension of uniform spheres under conditions of viscous flow. Chem. Eng. Sci. 3 (2), 65–73. https://doi.org/10.1016/0009-2509(54)85015-9.

Rietveld, L.C., 2005. Improving Operation of Drinking Water Treatment Through Modelling. Doctoral Dissertation, Delft University of Technology.

Schetters, M.J.A., Van der Hoek, J.P., Kramer, O.J.I., Kors, L.J., Palmen, L.J., Hofs, B., Koppers, H., 2015. Circular economy in drinking water treatment: reuse of ground pellets as seeding material in the pellet softening process. Water Sci. Technol. 71 (4), 479–486. https://doi.org/10.2166/wst.2014.494.

Schetters, M.J.A., 2013. Grinded Dutch calcite As Seeding Material in the Pellet Softening Process. Master Thesis. Delft University of Technology, Department of Civil Engineering and Geosciences.

Seepma, S.Y.M.H., Ruiz-Hernandez, S.E., Nehrke, G., Soetaert, K., Philipse, A.P., Kuipers, B.W.M., Wolthers, M., 2021. Controlling $CaCO_3$ particle size with $\{Ca^{2+}\}$: $\{CO_3^{2-}\}$ ratios in aqueous environments. Cryst. Grow. Des. 21 (3), 1576–1590. https://doi.org/10.1021/acs.cgd.0c01403.

Seepma, S.Y.M.H., Koskamp, J.A., Colin, M.G., Chiou, E., Sobhan, R., Bögels, T.F.J., Bastiaan, T., Zamanian, H., Baars, E.T., De Moel, P.J., Wolthers, M., Kramer, O.J.I., 2025. Mechanistic model advancements for optimal calcium removal in water treatment: integral operation improvements and reactor design strategies. Water Res. 268 (pt. B), 122781. https://doi.org/10.1016/j.watres.2024.122781.

Smoluchowski, M., 1916. Drei Vorträge über diffusion, Brownsche molekularbewegung und koagulation von Kolloidteilchen. Phisik. Z. 17, 585–599.

Sobhan, R., 2019. An Improved Kinetic Model and Optimized Configurations For Pellet softening: Modeling and Optimization of Pellet Softening Process in Drinking Water

Treatment. Master Thesis. Delft University of Technology, Department of Civil Engineering and Geosciences.
Tang, C., Hedegaard, M.J., Lopato, L., Albrechtsen, H.-J., 2019. Softening of drinking water by the pellet reactor – Effects of influent water composition on calcium carbonate pellet characteristics. Sci. Total Environ. 652, 538–548. https://doi.org/10.1016/j.scitotenv.2018.10.157.
Towler, G., Sinnott, R., 2021. Chemical Engineering design: principles, Practice and Economics of Plant and Process Design, 3rd ed. Butterworth-Heinemann, Kidlington, UK. https://doi.org/10.1016/C2019-0-02025-0.
Van der Bruggen, B., Goossens, H., Everard, P.A., Stemgée, K., Rogge, W., 2009. Cost-benefit analysis of central softening for production of drinking water. J. Environ. Manage. 91 (2), 541–549. https://doi.org/10.1016/j.jenvman.2009.09..024.
Van Schagen, K.V., Rietveld, L.C., Babuška, R., 2008. Dynamic modelling for optimisation of pellet softening. J. Water Supply: Res. Technol. – AQUA 57 (1), 45–56. https://doi.org/10.2166/aqua.2008.097.
Van Schagen, K.M., 2009. Model-based Control of Drinking-Water Treatment Plants. Doctoral Dissertation, Delft University of Technology.
Watkinson, W.J., 2008. Chemistry of detergents and disinfectants. In: Tamime, A.Y. (Ed.), Cleaning-in-Place: Dairy, Food and Beverage Operations, 3rd ed. Blackwell Publishing, Oxford, UK, pp. 56–80. https://doi.org/10.1002/9781444302240.
Wiechers, H.N.S., Sturrock, P., Marais, G.V.R., 1975. Calcium carbonate crystallization kinetics. Water Res. 9 (9), 835–845. https://doi.org/10.1016/0043-1354(75)90143-8.
Wolthers, M., Nehrke, G., Gustafsson, J.P., Van Cappellen, P., 2012. Calcite growth kinetics: modeling the effect of solution stoichiometry. Geochim. Cosmochim. Acta 77, 121–134. https://doi.org/10.1016/g.gca.2011.11.003.
Wray, J.L., Daniels, F., 1957. Precipitation of calcite and aragonite. J. Am. Chem. Soc. 79 (9), 2031–2034. https://doi.org/10.1021/ja01566a001.
Zhang, L., Mishra, D., Zhang, K., Perdicakis, B., Pernitsky, D., Lu, Q., 2020. Electrokinetic study of calcium carbonate and magnesium hydroxide particles in lime softening. Water Res., 116415 https://doi.org/10.1016/j.watres.2020.116415.
Zhu, Y., Gao, Z., Lee, B., Jun, Y.S., 2022. Process-specific effects of sulfate on $CaCO_3$ formation in environmentally relevant systems. Environ. Sci. Technol. 56 (12), 9063–9074. https://doi.org/10.1021/acs.est.1c08898.